optica

Optical triangulations of curved spaces

Dimitris Georgantzis Garcia,[1,2] Gregory J. Chaplain,[1,3] Jakub Bělín,[1] Tomáš Tyc,[4] Christoph Englert,[1] and Johannes Courtial[1,*]

[1]School of Physics & Astronomy, University of Glasgow, Glasgow G12 8QQ, UK
[2]Current address: Sheffield University Management School, University of Sheffield, Conduit Road, Sheffield S10 1FL, UK
[3]Current address: Department of Mathematics, Imperial College London, London SW7 2AZ, UK
[4]Institute of Theoretical Physics and Astrophysics, Masaryk University, Kotlárská 2, 61137 Brno, Czech Republic
*Corresponding author: johannes.courtial@glasgow.ac.uk

Not only do curved spaces fascinate scientists and non-scientists, but they are also at the heart of general relativity and modern theories of quantum gravity. Optical systems can provide models for the wave and quantum behavior of curved spaces. Here we show how to construct optical systems that simulate triangulations of 3D curved spaces, for example, the curved 3D surface of a 4D hypersphere. Our work offers a new approach to the optical simulation of curved spaces, and has the potential to lead to new ways of thinking about physics in curved spaces and simulating otherwise inaccessible phenomena in non-Euclidean geometries.

1. INTRODUCTION

Physics in curved spaces and curved space–time is subject to extensive research. The basic properties of curvature can be seen in the standard example of a curved space: the two-dimensional (2D) surface of a sphere. In such spaces, very unusual phenomena can be observed, such as the sum of the inner angles of a triangle being different from π [Fig. 1(a)]—an example of *angular defect*, one of the hallmarks of curvature. Ever since Einstein's general theory of relativity [1], such spaces have been central to theories of gravity, including modern theories of quantum gravity such as string theory [2]. Many theoretical predictions of curved space–time physics, such as gravitational lensing [3], black holes [4], and gravitational waves [5], have been observed experimentally [6–9], but there are still phenomena that remain unobserved, e.g., the gravitational self-interaction of quantum wavepackets [10], Hawking radiation [11], the Unruh effect [12], and the compactified dimensions of Kaluza–Klein theory [13,14] and of string theory [2]. As such experiments "enable control over physical parameters, suggest new insights and offer considerable intuition" [15], several attempts have been made to simulate these inaccessible phenomena in the laboratory [15–19].

In 2D waveguides, light behaves as in a 2D space, and curved 2D waveguides have been used to simulate curved spaces [20–23]. Three-dimensional (3D) curved spaces cannot be simulated in this straightforward manner. However, in 1925, Tamm [24] discovered that light propagation in anisotropic media is equivalent to light propagation in gravitational fields in vacuum, which general relativity described as metric spaces; these ideas led directly to modern attempts to simulate optical phenomena in curved spaces

in metamaterial structures (e.g., [25–33]). Due to their manmade sub-wavelength structure, metamaterials can exhibit extraordinary properties not found naturally, but these properties often hold in only a very narrow wavelength range and are associated with significant absorption [34]; additionally, metamaterials can be difficult and costly to manufacture.

A curved smooth surface, such as the surface of a sphere, can be approximated by a surface comprising planar triangles [Fig. 1(b)]; smaller triangles allow the surface to be approximated more closely. In this piecewise triangular approximation of the curved surface, curvature is concentrated into the vertices of the triangles, and with it the angular defect, which now manifests as the angles completely surrounding the vertices on the surface adding up *not* to 2π (as they would if the surface was flat), but to $2\pi - \varepsilon$, where ε is the so-called *deficit angle*. This idea can be generalized to higher dimensions: in N dimensions, the triangles become N-simplices (tetrahedra in 3D), and curvature is concentrated into the $(N-2$-dimensional) edges of these simplices. This is the basis of Regge calculus [35], which discretizes the dynamics of space–time geometry using simplices, the generalization of triangles in any dimension, and which is used to numerically investigate aspects of general relativity, for instance, black hole collisions [36], whose relevance is particularly timely after the recent discovery of gravitational waves [37].

The angular deficit of a vertex can be visualized when the surface around the vertex is unwrapped into a plane [Fig. 1(c)]. The deficit angle ε then corresponds to a wedge of the same angle of "missing space." Conversely, a wedge of missing space corresponds to a corresponding deficit angle. In this paper, we discuss, theoretically, ways in which a wedge of space can be made to disappear optically
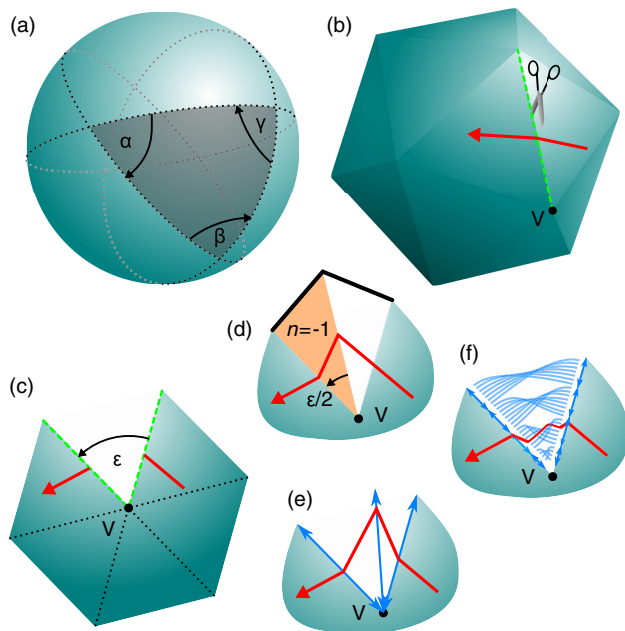
Fig. 1. Curved surface of a sphere (a) and its piecewise triangular approximation (b). In the geodesic triangle on the surface of the sphere, the sum of the inner angles, $\alpha + \beta + \gamma$, does not equal π, illustrating angular defect. In the piecewise triangular approximation, the angular defect is concentrated in the vertices. This can be seen by cutting the surface around a vertex, V, and unfolding it into a plane (c); the angular deficit is then visible as a wedge of missing space; the wedge angle, ε, is the deficit angle of the vertex. In this unfolding, the geodesic (red arrow) shown in (b) is cut into two parts that are rotated relative to each other by ε around V. (d) A combination of a wedge of material with refractive index $n = -1$ (shaded) and wedge angle $\varepsilon/2$ and mirrors (solid black lines), arranged as shown, rotates any light ray (red arrow) incident on the wedge by an angle ε around V. It therefore redirects light rays such that they travel along geodesics in the unfolded space shown in (c). Alternative ways to redirect light rays in this manner include combinations of skew lenses (azure double-sided arrows) (e) and light-field transfer using arrays of lenslets (azure double-sided arrows) and coherent fiber bundles (azure lines) (f).

using a device we call a "space-canceling (SC) wedge." We discuss several designs for such SC wedges, some easier to realize than others [Figs. 1(d)–1(f)]. We then show how to combine such SC wedges into meaningful curved spaces. We show how to combine SC wedges into the 2D surfaces corresponding to the simplest triangulations of the surface of a sphere, namely, the surface of a tetrahedron and a cube. More interestingly, we also combine them into the 3D surfaces of a four-dimensional (4D) tetrahedron (also known as four-simplex and five-cell) and of a 4D hypercube (tesseract). Finally, we discuss different aspects of this work, including the problem of negative curvature, before concluding.

2. CONSTRUCTING A SPACE-CANCELING WEDGE

A key ingredient of our construction is an optical device for removing a wedge of optical space: a SC wedge. This requires a device that optically identifies two intersecting half-planes with each other, which is achieved by bringing light rays entering the device through one plane to the corresponding position on the other

plane, rotating each ray around the intersection line by the intersection angle, ε. We describe here four ways to achieve this, all of which are discussed in more detail in Supplement 1.

One approach employs a material with negative refractive index. It is well known that a uniform layer of a material with refractive index $-n$ can "cancel" another equally thick layer of material with refractive index $+n$ [38,39]. In a similar way, a negatively refracting wedge of space can optically "cancel" a wedge of positive refractive index [Fig. 1(d)]. The addition of two mirrors (in 2D) or four mirrors (in 3D) makes this structure work for all light-ray directions (see Supplement 1, Section 1). Practical realization requires, over a suitable bandwidth, bulk materials with negative refractive index, ideally $n = -1$, and low loss. Building such a material is very difficult, perhaps even impossible, but promising progress is being made using active materials [40,41].

A second approach avoids negative refraction but, in general, requires inhomogeneous and anisotropic materials. It starts from one half of a suitable Lissajous lens [42], a refractive-index distribution that is restricted to one side of a plane and that images two halves of that plane into each other such that the image position and the direction of any ray are rotated by π around the line dividing the plane. It consists entirely of isotropic materials and acts as a SC wedge with deficit angle π. Other deficit angles can be achieved by making this device the virtual space of a transformation-optics device [43,44] that maps the wedge of wedge angle π containing the device into a wedge with the required wedge angle ε. The resulting wedge of anisotropic material is a SC wedge with deficit angle ε. Note that even though this approach avoids negative refraction, it still suffers from the limitations (such as the narrow wavelength range and significant absorption) and manufacturing difficulty and cost of the standard metamaterials approach. Details can be found in Supplement 1, Section 2.

The third approach uses skew ideal lenses [Fig. 1(e)]. In theory, combinations of three skew ideal lenses that intersect in a line can create an image that is rotated by an arbitrary angle around the lenses' intersection line [45] (see Supplement 1, Section 3). In practice, however, ideal thin lenses cannot currently be realized physically, although metalenses [46–48] are getting closer. Furthermore, the ideal-lens combinations rotate only light rays that pass through all three lenses, but in all combinations investigated to date, this is the case only over a limited field of view. Nevertheless, this approach provides hope that optical simulations of curved spaces can be performed using mere lenses, optical instruments thought to have existed for more than 2700 years [49].

The fourth, and perhaps easiest to realize, approach transfers the light field [50] from one face of the SC wedge to the other. This can be done by using an array of optical fibers to connect the focal planes of two lenslet (or microlens) arrays [Fig. 1(f)]. Depending on which lenslet L_1 in the first array an incident light ray passes through, and the direction with which it is incident, the light ray is directed by L_1 into one particular fiber. After the ray exits the fiber's other end and passes through the lenslet in the second array that corresponds to L_1, it has the required direction. Light rays can also pass through the device in reverse. The two lenslet arrays then act like the faces of a SC wedge in which both positions and directions are discretized, and the space-bandwidth product of the device correspondingly limited.

3. SIMULATING CURVED 2D SPACES

SC wedges can be fitted together in a meaningful manner. First, we give a general description of our approach for the 2D situation, i.e., for curved 2D surfaces. We demonstrate our method on specific examples that help to understand it more intuitively. As examples, we choose to construct the simplest symmetrical triangulations of the surface of a sphere, namely, surfaces of the tetrahedron and the cube. These are the two simplest Platonic solids (all their faces are identical regular polyhedra), and their surfaces are, of course, 2D curved spaces. Later, in the next section, we will then extend our construction to 3D hypersurfaces of 4D polyhedra.

As the first step, we construct the 2D surface (call it S) of a closed 3D polyhedron (call it P) from a plane. This can be done employing a *net N* of the surface S, which is simply an unfolded form of that surface. The net has to be accompanied by appropriate gluing instructions that determine which pairs of edges of the net have to be identified with one another; such a space with gluing instructions is also called a quotient space [51]. The net N can then be folded and "glued" to become the surface S.

The procedure is made clearer by inspecting specific examples. We start by constructing the surface of a tetrahedron [Fig. 2(a)], which can be unfolded [Fig. 2(b)] into its net, an equilateral triangle [Fig. 2(c)]. The appropriate gluing is such that each half of each edge is identified with the other half of the same edge, with each midpoint of the edges becoming a different vertex and the three vertices of the net meeting at the same point to become the fourth vertex, V, of the tetrahedron. Similarly, other polyhedra can be unfolded; Figs. 2(d)–2(f) show a symmetric unfolding of a cube.

To simulate light propagation on the surface of a polyhedron, we let light propagate on its unfolded net, identifying the corresponding edges optically. This is done by removing the appropriate wedges of space. Figure 2(g) shows the net of a tetrahedron realized in this way. Three SC wedges each cancel an angle π, outlining the net of the tetrahedron. We ran a raytracing simulation of our setup, with three different light-ray trajectories, also shown in Fig. 2(g). The net of the tetrahedron in Fig. 2(g) (the large triangle, without the SC wedges) can be printed and folded to form the tetrahedron; this results in continuous light-ray trajectories that correspond to the desired geodesics on the surface of a tetrahedron [Fig. 2(h)]. Figure 2(j) and 2(k) show the equivalent for the net of a cube.

Figures 2(i) and 2(l) show virtual views of observers respectively living on the surface of a tetrahedron and of a cube. However, to be able to demonstrate the features of such a view, we have added a third dimension perpendicular to the surface; the resulting 3D space is a tensor product of the 2D surface and one-dimensional Euclidean space $\mathbb{R}$. Without this added dimension, the image would have to be one-dimensional, without much information content. We have also inserted a ball into this space for the observer to look at. Due to the finite size of the surface, observers see many copies of the ball corresponding to many different rays from the ball to their eyes.

4. SIMULATING CURVED 3D SPACES

Having explained how to simulate (and in principle demonstrate) light propagation in a 2D curved space, we include an additional dimension. To this end, consider a 4D polyhedron P. Its hypersurface S is three-dimensional and composed of faces, which are 3D polyhedra. In a similar way as described in the previous section, we can construct the net N of P, which will be a composition of 3D polyhedra with the appropriate gluing instructions, which identify pairs of 2D faces of these 3D polyhedra with one another. If we are able to insert the appropriate SC wedges that transfer light between the two 2D faces to be identified in each pair, then light propagation in this structure will be the same as light propagation on a real 3D hypersurface of the 4D polyhedron.

This can indeed be done for the simplest 4D polyhedron, the so-called five-cell or four-simplex. This object can be obtained from a 3D tetrahedron by adding an extra vertex to it (lying outside the 3D space of the tetrahedron, in the fourth dimension) and connecting it with all four vertices of the tetrahedron. There will be five 3D faces of the resulting five-cell, one originating from each triangular face of the original tetrahedron, plus the original tetrahedron itself [52].

It is not difficult to construct the net of the five-cell. All five faces are tetrahedra, so the net consists of an inner tetrahedron that has a tetrahedron stuck to each one of its triangular faces [see Fig. 3(a)]. Folding this net into the fourth dimension such that all the outer vertices coincide without tearing the net then constructs the five-cell. This procedure is hard to picture by the human brain, as we experience only three spatial dimensions. However, this "folding without tearing" can be done optically by constructing the net of the five-cell and employing six SC wedges, each edge of the inner tetrahedron being the tip of one SC wedge. In the case of a regular five-cell, which is composed exclusively of regular tetrahedra, since the dihedral angle (the angle between neighboring faces) of a regular tetrahedron is $\alpha = \tan^{-1}(2\sqrt{2})$, each SC wedge should cancel an angle $\varepsilon = 2\pi - 3\alpha \approx 2.59$ rad.

Raytracing simulations of this setup are shown in Figs. 3(b) and 3(d). Figure 3(b) shows the unfolded net with a light-ray trajectory that follows a geodesic in this space. Figure 3(d) shows the view on the hypersurface S by an observer also located in S. A white sphere has been placed in S, as shown in Fig. 3(c).

Similarly, the net of a hypercube can be simulated [see Fig. 3(e)]. Figure 3(f) shows a light-ray trajectory in this net; Fig. 3(g) shows the net with a sphere placed inside it, and Fig. 3(h) shows a ray-tracing simulation of the view on the hypersurface (including the sphere) by an observer located in the center of the net.

5. DISCUSSION

Our method of simulating light propagation on the surface of a polyhedron by unfolding it into the net closely resembles the concept of non-Euclidean transformation optics [26]. There, one starts from non-Euclidean virtual space (e.g., the surface of a sphere attached to a plane), which is mapped to physical space (e.g., a plane). The map between the two spaces induces a refractive index profile in physical space, and light is directed by this profile to follow lines that correspond to geodesics in virtual space.

Interestingly, we can think of the surface of the polyhedron P as described earlier as a non-Euclidean virtual space, and regard the quotient space (i.e., the unfolded net along with the gluing instructions) as physical space. Physical space might appear flat at first sight; however, due to identifying the pairs of edges (and hence eliminating the deficit angles), it is not flat at the vertices of the quotient space—the curvature is concentrated exactly at these vertices. This introduces a new concept into transformation optics, extending its ideas and capabilities.
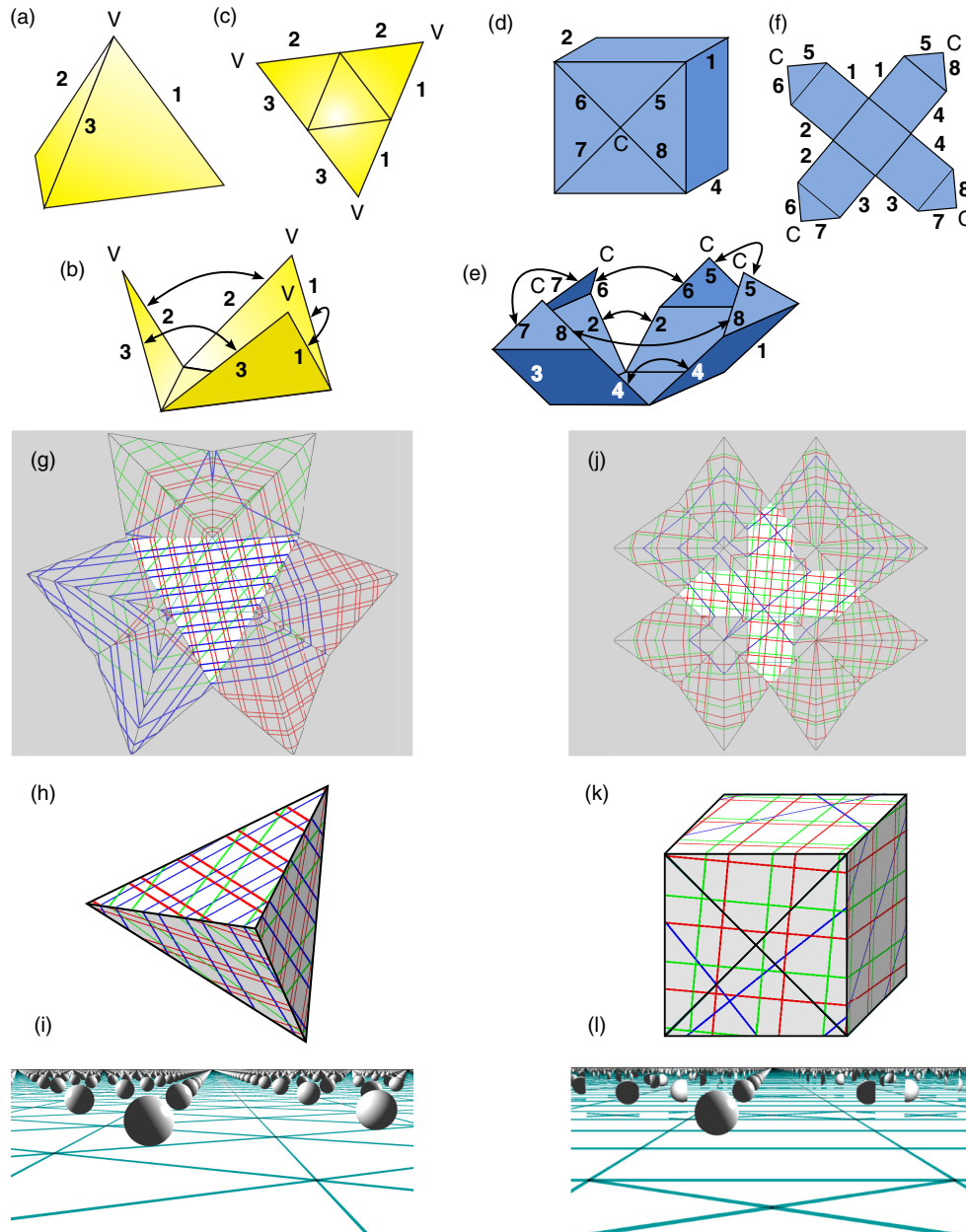
Fig. 2.   Optical simulation of the surface of a regular tetrahedron and a cube. Unfolding of the surface of a regular tetrahedron (a) and of a cube (d) into the respective nets (c) and (f). (b), (e) Intermediate stages of unfolding. Edges labeled with the same number are identified ("gluing instructions"); in (b) and (e), arrows indicate how each of these edges of the surface splits into two edges in the equivalent net. V is the fourth vertex of the tetrahedron; in the unfolded and partially folded net, it appears as three separate vertices. To achieve a symmetric unfolding, one of the cube faces has been divided into four right triangles; C is the center of that face. (g), (j) Instead of mechanically folding the net and gluing corresponding edges together, corresponding edges are "optically glued," i.e., imaged, by SC wedges. Rays trace out geodesics on this (optically glued) surface; three rays (red, green, blue) are shown in each case. (h), (k) Mechanical folding and gluing of the net and the simulated ray trajectories confirm that the trajectories are continuous. (i), (l) Photorealistic simulation of the view of a white sphere on a surface as seen from within the surface, with an added third, Euclidean, dimension perpendicular to the surface. The cyan lines show the edges of the tetrahedron and the cube, respectively. Details of the raytracing simulations can be found in Supplement 1, Section 5.

Note that in this paper we have simulated only positive deficit angles, corresponding to curved spaces with positive (Gauss) curvature. This was done by "canceling" a wedge of space with an angle ε at the tip. However, there exist also spaces with negative Gauss curvature, the prime example being the pseudosphere [53]. A question then arises as to whether our method can be adapted to such spaces as well. It seems to be difficult because instead of "canceling" a part of space, we would have to "add" a wedge of space to the edge. One idea is to create two SC wedges with positive deficit angles, ε_1 and ε_2, and then map each edge of one SC wedge into a corresponding wedge of the other SC wedge such that the tips are mapped into each other, and therefore optically identified. This would result in a single apparent SC wedge in which the angles of (non-canceled) space of the two constituent SC wedges, $2\pi - \varepsilon_1$ and $2\pi - \varepsilon_2$, add up, resulting in a deficit angle that can be positive or negative; the next challenge is to combine such apparent SC wedges into meaningful spaces.
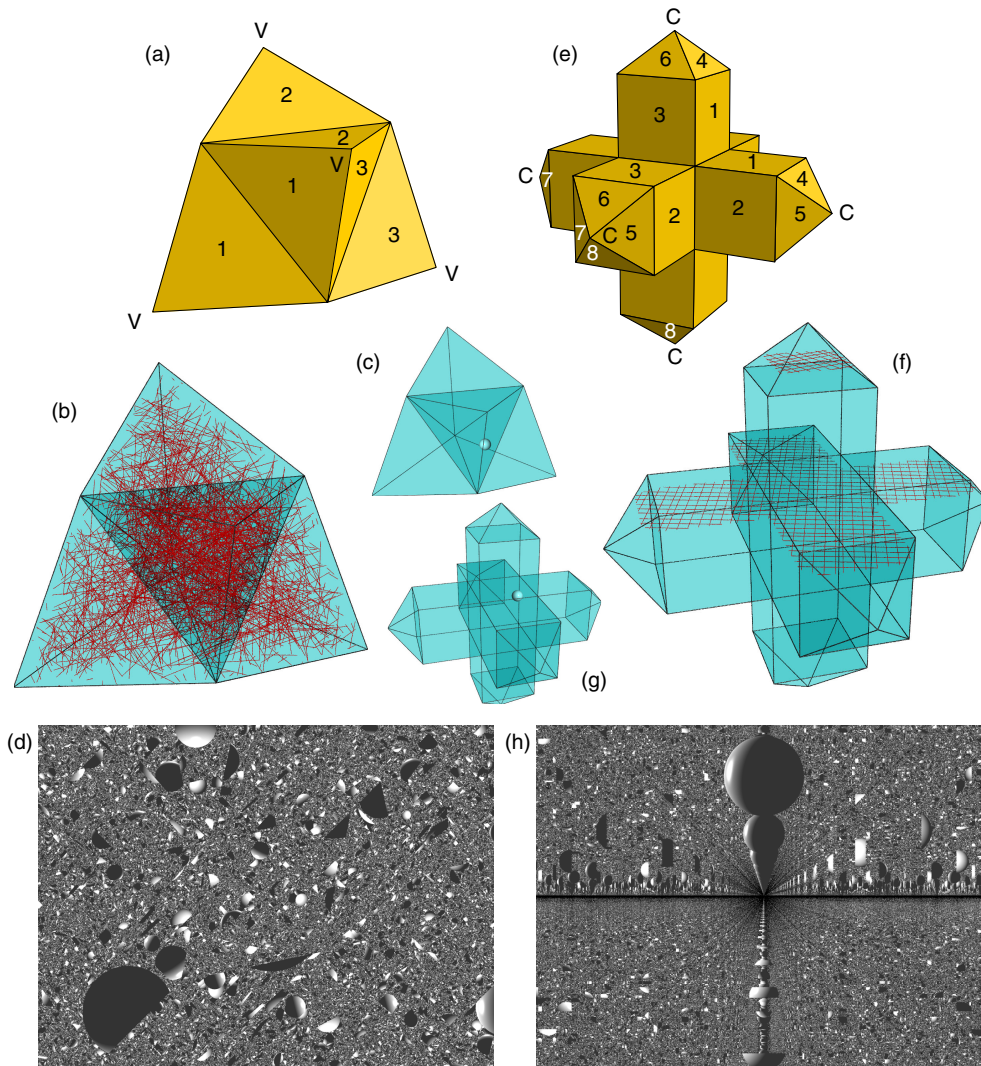
Fig. 3.   Raytracing simulations of the 3D hypersurface of a five-cell (left) and of a hypercube (right). (a), (e) Gluing instructions: faces with the same numbers are identified; in unnumbered faces, the identified face is not visible. (a) Four outermost vertices, labeled V, are identified; after folding, they form the fifth vertex of the five-cell. In the case of the hypercube (e), the four outermost vertices, all labeled C, are identified, forming the center of the eighth cubic cell of the hypercube. (b) One light-ray trajectory (red line) is shown from the outside of the net. The view from within the hypersurface is shown in (d), where a white sphere has been placed within the space as shown in (c). (f), (g), (h) Similar simulations have also been performed for the hypercube. See Section 5 of Supplement 1 for details of the raytracing simulations.

6. CONCLUSION

In this paper, we have demonstrated a new approach for the optical simulation of curved spaces. As examples of curved 2D surfaces we have used surfaces of simple platonic bodies that can be seen as piecewise flat approximations to the surface of a sphere. We have also extended our approach to 3D hypersurfaces of 4D polyhedra, namely, the five-cell and the hypercube. To do this, we have employed a mechanism that connects the edges or faces to be glued. This can be achieved by using either wedges of negative refractive index (or ray-optical approximations thereof), or a combination of absolute optical instruments modified by the methods of transformation optics. For concave polyhedra, it would be difficult to perform the optical gluing physically; however, light propagation even on such surfaces can be visualized using numerical simulations.

Experimental simulations of curved spaces "suggest new insights and offer considerable intuition" [15], and we hope that

our ideas also have this effect, with or without experimental realization. In fact, inspired by this research, a few of us have already started to investigate wave optics and quantum motion on the surface of polyhedra [54]. We hope that our work will open up further new possibilities in the exciting field of light propagation in curved spaces, a field at the crossing of transformation optics, negative refraction, geodesic lenses, absolute optical instruments, general relativity, and quantum gravity.

The ability to realize such systems experimentally would enable optical simulations of wave mechanics and quantum mechanics [55] in such spaces. Although we have used elements of Regge calculus in this paper to purely realize optical curvature, the relation to gravity is evident. Localized solutions of general relativity such as cosmic strings and their related dynamics have motivated laboratory tests employing metamaterials, see, e.g., [30,32]. The methodology outlined and demonstrated in this work provides a new and complementary approach along these lines.

REFERENCES

1. A. Einstein, "Die Grundlage der allgemeinen Relativitätstheorie," Ann. Phys. **354**, 769–822 (1916).
2. K. Becker, M. Becker, and J. H. Schwarz, *String Theory and M-Theory. A Modern Introduction* (Cambridge University, 2007).
3. A. Einstein, "Lens-like action of a star by the deviation of light in the gravitational field," Science **84**, 506–507 (1936).
4. K. Schwarzschild, "Über das Gravitationsfeld eines Massenpunktes nach der Einsteinschen Theorie," in *Sitzungsberichte der Königlich Preussischen Akademie der Wissenschaften* (Verlag der Königlichen Akademie der Wissenschaften, 1916), pp. 189–196.
5. A. Einstein and N. Rosen, "On gravitational waves," J. Franklin Inst. **223**, 43–54 (1937).
6. D. Walsh, R. F. Carswell, and R. J. Weymann, "0957+ 561 A, B: twin quasistellar objects or gravitational lens?" Nature **279**, 381–384 (1979).
7. C. T. Bolton, "Identification of Cygnus X-1 with HDE 226868," Nature **235**, 271–273 (1972).
8. B. P. Abbott, LIGO Scientific Collaboration, and Virgo Collaboration, "Observation of gravitational waves from a binary black hole merger," Phys. Rev. Lett. **116**, 061102 (2016).
9. The Event Horizon Telescope Collaboration, "First M87 event horizon telescope results. I. The shadow of the supermassive black hole," Astrophys. J. Lett. **875**, 1–17 (2019).
10. R. Penrose, "On gravity's role in quantum state reduction," Gen. Relat. Gravit. **28**, 581–600 (1996).
11. S. W. Hawking, "Black hole explosions?" Nature **248**, 30–31 (1974).
12. W. G. Unruh, "Notes on black-hole evaporation," Phys. Rev. D **14**, 870–892 (1976).
13. T. Kaluza, "Zum Unitätsproblem in der Physik," in *Sitzungsber. Preuss. Akad. Wiss.* (1921), pp. 966–972.
14. O. Klein, "Quantentheorie und fünfdimensionale Relativitätstheorie," Z. Physik **37**, 895–906 (1926).
15. R. Bekenstein, R. Schley, M. Mutzafi, C. Rotschild, and M. Segev, "Optical simulations of gravitational effects in the Newton-Schrödinger system," Nat. Phys. **11**, 872–878 (2015).
16. C. Barceló, S. Liberati, and M. Visser, "Probing semiclassical analog gravity in Bose-Einstein condensates with widely tunable interactions," Phys. Rev. A **68**, 053613 (2003).
17. T. G. Philbin, C. Kuklewicz, S. Robertson, S. Hill, F. König, and U. Leonhardt, "Fiber-optical analog of the event horizon," Science **319**, 1367–1370 (2008).
18. F. Belgiorno, S. L. Cacciatori, M. Clerici, V. Gorini, G. Ortenzi, L. Rizzi, E. Rubino, V. G. Sala, and D. Faccio, "Hawking radiation from ultrashort laser pulse filaments," Phys. Rev. Lett. **105**, 203901 (2010).
19. J. B. Pendry, P. A. Huidobro, Y. Luo, and E. Galiffi, "Compacted dimensions and singular plasmonic surfaces," Science **358**, 915–917 (2017).
20. G. C. Righini, V. Russo, S. Sottini, and G. T. di Francia, "Geodesic lenses for guided optical waves," Appl. Opt. **12**, 1477–1481 (1973).
21. V. H. Schultheiss, S. Batz, A. Szameit, F. Dreisow, S. Nolte, A. Tünnermann, S. Longhi, and U. Peschel, "Optics in curved space," Phys. Rev. Lett. **105**, 143901 (2010).
22. C. Sheng, H. Liu, Y. Wang, S. N. Zhu, and D. A. Genov, "Trapping light by mimicking gravitational lensing," Nat. Photonics **7**, 902–906 (2013).
23. R. Bekenstein, Y. Kabessa, Y. Sharabi, O. Tal, N. Engheta, G. Eisenstein, A. J. Agranat, and M. Segev, "Control of light by curved space in nanophotonic structures," Nat. Photonics **11**, 664–670 (2017).
24. I. E. Tamm, "Crystal-optics of the theory of relativity pertinent to the geometry of a biquadratic form," J. Russ. Phys. Chem. Soc. **57**, 209 (1925).
25. A. Greenleaf, Y. Kurylev, M. Lassas, and G. Uhlmann, "Electromagnetic wormholes and virtual magnetic monopoles from metamaterials," Phys. Rev. Lett. **99**, 183901 (2007).
26. U. Leonhardt and T. Tyc, "Broadband invisibility by non-Euclidean cloaking," Science **323**, 110–112 (2009).
27. D. A. Genov, S. Zhang, and X. Zhang, "Mimicking celestial mechanics in metamaterials," Nat. Phys. **5**, 687–692 (2009).
28. I. I. Smolyaninov and E. E. Narimanov, "Metric signature transitions in optical metamaterials," Phys. Rev. Lett. **105**, 067402 (2010).
29. H. Chen, R.-X. Miao, and M. Li, "Transformation optics that mimics the system outside a Schwarzschild black hole," Opt. Express **18**, 15183–15188 (2010).
30. T. G. Mackay and A. Lakhtakia, "Towards a metamaterial simulation of a spinning cosmic string," Phys. Lett. A **374**, 2305–2308 (2010).
31. T. G. Mackay and A. Lakhtakia, "Towards a piecewise-homogeneous metamaterial model of the collision of two linearly polarized gravitational plane waves," IEEE Trans. Antennas Propag. **62**, 6149–6154 (2014).
32. T. G. Mackay and A. Lakhtakia, "Metamaterial models of curved spacetime," Proc. SPIE **9544**, 95442K (2015).
33. I. Fernández-Núñez and O. Bulashenko, "Anisotropic metamaterial as an analogue of a black hole," Phys. Lett. A **380**, 1–8 (2016).
34. N. I. Zheludev, "The road ahead for metamaterials," Science **328**, 582–583 (2010).
35. T. Regge, "General relativity without coordinates," Nuovo Cimento **19**, 558–571 (1961).
36. A. P. Gentle, "Regge calculus: a unique tool for numerical relativity," Gen. Relat. Gravit. **34**, 1701–1718 (2002).
37. B. P. Abbott, LIGO Scientific Collaboration, and Virgo Collaboration, "GW170817: observation of gravitational waves from a binary neutron star inspiral," Phys. Rev. Lett. **119**, 161101 (2017).
38. V. G. Veselago, "The electrodynamics of substances with simultaneously negative values of ε and μ," Sov. Phys. Uspekhi **10**, 509–514 (1968).
39. J. B. Pendry and S. A. Ramakrishna, "Focusing light using negative refraction," J. Phys. Condens. Matter **15**, 6345–6364 (2003).
40. S. Wuestner, A. Pusch, K. L. Tsakmakidis, J. M. Hamm, and O. Hess, "Overcoming losses with gain in a negative refractive index metamaterial," Phys. Rev. Lett. **105**, 127401 (2010).
41. D. Ye, K. Chang, L. Ran, and H. Xin, "Microwave gain medium with negative refractive index," Nat. Commun. **5**, 5841 (2014).
42. A. J. Danner, H. L. Dao, and T. Tyc, "The Lissajous lens: a three-dimensional absolute optical instrument without spherical symmetry," Opt. Express **23**, 5716–5722 (2015).
43. J. B. Pendry, D. Schurig, and D. R. Smith, "Controlling electromagnetic fields," Science **312**, 1780–1782 (2006).
44. U. Leonhardt and T. G. Philbin, "General relativity in electrical engineering," New J. Phys. **8**, 247 (2006).
45. J. Bělín, G. Ferenczi, and J. Courtial, "Ideal-lens image rotator," (submitted).
46. W. T. Chen, A. Y. Zhu, V. Sanjeev, M. Khorasaninejad, Z. Shi, E. Lee, and F. Capasso, "A broadband achromatic metalens for focusing and imaging in the visible," Nat. Nanotechnol. **13**, 220–226 (2018).
47. S. Shrestha, A. C. Overvig, M. Lu, A. Stein, and N. Yu, "Broadband achromatic dielectric metalenses," Light Sci. Appl. **7**, 85 (2018).
48. M. Khorasaninejad, W. T. Chen, R. C. Devlin, J. Oh, A. Y. Zhu, and F. Capasso, "Metalenses at visible wavelengths: diffraction-limited focusing and subwavelength resolution imaging," Science **352**, 1190–1194 (2016).
49. The British Museum, "Collection online. The Nimrud Lens/The Layard Lens," https://research.britishmuseum.org/research/collection_online/collection_object_details.aspx?objectId=369215&partId=1.
50. E. H. Adelson and J. R. Bergen, "The plenoptic function and the elements of early vision," in *Computational Models of Visual Processing*, M. Landy and J. A. Movshon, eds. (MIT Press, 1991), pp. 3–20.
51. S. E. Goodman, *Beginning Topology* (American Mathematical Society, 2005), chap. 2.3.
52. N. W. Johnson, *Geometries and Transformations* (Cambridge University, 2018).
53. T. Needham, *Visual Complex Analysis* (Clarendon, 2000).
54. J. Bělín, S. A. R. Horsley, and T. Tyc, "Quantum mechanics and Talbot revivals on a tetrahedron," Phys. Rev. A **100**, 033806 (2019).
55. J. I. Cirac and P. Zoller, "Goals and opportunities in quantum simulation," Nat. Phys. **8**, 264–266 (2012).